Two-Stage Dust Removal System for Mars In-Situ Resource Utilization Systems: System Sizing and Trade-offs

Ariane B. Chepko[1] and Michael E. Swanwick[2]
Creare LLC, Hanover, NH, 03766

Paul H. Sorensen[3]
Shell TechWorks, Cambridge, MA, 02139

Darius Modarress[4]
Measurement Science Enterprise, Inc, Pasadena, CA, 91105

A two-stage dust filtration system is presented for Mars in situ resource utilization (ISRU) gas processing systems consisting of a cyclone pre-filter and an electrostatic precipitator (ESP). An inertial cyclone pre-filter upstream of the ESP offers a regenerable, passive, and robust approach to capture the larger particles and reduce the required size of the ESP stage. We present the development of a system model to estimate performance of a cyclone-ESP dust separator operating under low-pressure, Martian conditions. We compare the model to experimental cyclone tests and computational fluid dynamics (CFD) analysis, and estimate the performance and scalability of a two-stage dust separation system. We present the sizing and collection efficiency trade-offs between the stages for a validation-class ISRU processing system.

Nomenclature

A	=	ESP collection area
CFD	=	computational fluid dynamics
d	=	particle diameter
ESP	=	electrostatic precipitator
E	=	electric field strength
ISRU	=	in situ resource utilization
j	=	current flux
K	=	overall pressure drop coefficient
k_{in}	=	inlet pressure drop coefficient
ρ	=	gas density
P	=	pressure
Q_p^∞	=	saturation charge of particle
Q_p	=	charge of particle
RSM	=	Reynolds stress equation model
S	=	Sutherland constant
T	=	temperature
TSDS	=	two-stage dust separation system
v	=	average exit velocity
U	=	outlet tangential velocity
$\dot{V}$	=	gas volumetric flow rate
w	=	particle drift velocity

---

[1] Engineer, Creare LLC, abc@creare.com
[2] Engineer, Creare LLC, swanwick@creare.com
[3] Systems Engineering Fellow, Shell Techworks, p.sorensen@shell.com
[4] CTO, MSE Inc., DM@Measurementsci.com

λ	=	mean free path
ε_r	=	particle relative permittivity
ε_0	=	vacuum permittivity
η	=	collection efficiency
τ_Q	=	time constant for particle charging

I. Introduction

As NASA lays plans for future robotic and human exploration missions to Mars, one key technical challenge that must be overcome is the contamination of Martian dust into gas processing systems and human habitats. Dust can pose a serious threat to the operation and lifetime of mechanical systems and is a health hazard to crew should it enter the habitat. Conventional filters clog over time, requiring either frequent replacement or very large designs that accommodate end-of-life performance. One concept that has been explored for dust mitigation for in situ resource utilization (ISRU) atmospheric processing systems is an electrostatic precipitator (ESP).[1,2,3] This method can achieve high particle collection efficiency with low pressure drops. However, the low atmospheric pressures on Mars limit the electric field that can be employed in a Martian-based ESP and reduces collection efficiency for larger particles. An inertial cyclone pre-filter upstream of the ESP offers a regenerable, passive, and robust approach to capture the larger particles and reduce the required size of the ESP stage. We present the development of a two-stage dust separation system (TSDS) for Mars ISRU plants that combines the strengths of each filtration method to provide high-efficiency separation and minimize overall system size (Figure 1). We will discuss the development of an analytical system model to predict performance of each stage, low-pressure cyclone experiments, and the system-level sizing and trade-offs of this approach.
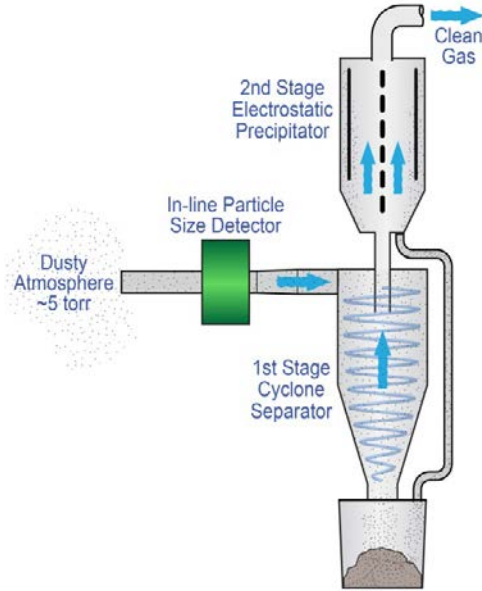

Figure 1. A two-stage dust separation system for Mars ISRU. *Combining a cyclone and ESP achieves ~99% separation of particles > 0.3 μm from the gas stream and minimizes system volume and power.*

Dust is permanently present in the Martian atmosphere. The mechanisms for dust entrainment are not fully understood and to date have not been directly measured. Existing measurements of the dust particle size and concentration have mainly been limited to indirect optical measurements that examine the bulk atmosphere (such as the LIDAR instrument on the Mars Phoenix lander).[4] The results of these measurements estimate an average suspended particle size of ~1.2 to 1.4 μm at a number density in the range of 3.2 to 4.4 cm^{-3}. Most models estimate that the density of particles in the atmosphere greater than 10 μm is very low, but estimates of the maximum particle size near ground level that may be partially entrained from saltation or dust devil activity vary from 20 to ~50 μm and higher. Though no direct measurements have been made to characterize dust electrostatic charge, it is theorized that triboelectrification of Martian dust contributes to its suspension in the atmosphere. While not a direct analog, initial electrostatic tests on Mars simulant (JSC Mars-1) show that simulant particles can be electrostatically charged.[5] Because it is certain that ISRU and habitation systems will encounter airborne dust on Mars, hardware must be designed to be robust to dust or to first separate dust from process gasses and the cabin environment.

ISRU plants for Mars use chemical conversion reactors, such as solid oxide electrolysis, to convert the CO_2 derived from the Martian atmosphere into oxygen. In order to feed these systems, the low-pressure CO_2 from the atmosphere must be acquired and compressed to close to Earth-atmospheric pressure. For the Mars 2020[6] technology demonstration, NASA's goal is to produce 22 g of O_2 per hour for 50 sol, whereas a human mission production plant would need to produce 2.2 kg of O_2 per hour for 500 sol. A stoichiometric calculation shows that the technology demonstrator mission will require 60.4 g of CO_2 per hour. Accounting for conversion efficiencies and losses, it is estimated that 90 g of CO_2 per hour will be required. For a human mission, 9 kg of CO_2 per hour will be required (Table 1). This mass flow rate corresponds to an inlet volumetric flow rate of 155 L/sec at Martian pressures. Many approaches to generating these flows are being explored, but most require some form of blower or

compressor to generate motive flow. Because the atmospheric pressure is so low, upstream components such as dust filters must impose a minimal pressure drop to avoid impacting blower performance; at the same time, overall system mass, volume, and power also must be considered. The goal of this development was to produce a dust filtration system that can achieve separation performance of 99% collection efficiency for ≥ 0.3 μm particles with less than 2 torr of pressure drop, based on NASA-specified requirements.

Table 1. ISRU plant capabilities for Mars 2020 and future exploration missions.			
	Mars 2020 Demonstration-Class Mission	Subscale Validation-Class Mission	Future Human Mission
Minimum Oxygen Production Rate	20 g/hr	440 g/hr	2200 g/hr
Minimum Operational Life	50 sols	500 sols	1200 sols
Estimated CO_2 Feedstock Rate	90 g/hr (0.8 SLPM[*])	1,800 g/hr (15.4 SLPM[*])	9,000 g/hr (76.9 SLPM[*])
[*]STP = 0°C at 10^5 Pa			

II. Two-Stage Dust Separation

The TSDS combines two common industrial dust separation techniques: an inertial cyclone separator and electrostatic precipitation. The first stage of the TSDS consists of an inertial cyclone separator that targets collection of 90% of particles greater than 1 μm. Cyclones direct incoming, dust-laden gas into a vortex flow. The induced centrifugal force carries the entrained particles to the wall, where friction slows them enough to fall out of suspension and into a collection hopper. Cyclones are most effective at separating larger particles, are robust with no moving parts, and can be periodically emptied of collected particulate by simply opening a gate valve. They have been demonstrated in reduced-gravity environments and can be designed to be orientation independent.[7] Our modeling of the full separator system revealed that maximizing the efficiency of the cyclone at collecting smaller particles will greatly reduce the required size of the second-stage ESP. Our testing with a cyclone prototype and our modeling effort indicate that achieving high separation efficiencies of down to 1 μm size particles within a ~1 torr pressure drop is feasible.

The second stage of the dust separator system consists of an ESP. In ESPs, dust particles are charged in a corona discharge by a biased electrode, and they then migrate to an oppositely charged collection plate electrode. The collection electrode is periodically vibrated to remove the discharged, collected dust into a hopper. Because the applied electric field force acts directly on the particles and there is no need to accelerate the gas phase to achieve separation, ESPs are characterized by having a low pressure drop. ESPs can achieve very high separation efficiencies. The shortcomings of ESPs are (1) their effectiveness depends on the resistivity of the dust, (2) large particle concentrations reduce separation efficiency or require larger electrode surface area, and (3) cleaning the electrodes of collected particles can be difficult. Applying this technology in a Martian environment adds the challenge that the breakdown voltage at Martian atmospheric pressure is relatively low, limiting the strength of the electric field that can be used to induce migration of the particles to the collector plates. This limits a Martian ESP's collection efficiency for larger particles. Despite these limitations, the ESP is still very attractive to use as a second-stage separator because the collection efficiency of the submicron particles is greater than 99% and the pressure drop is very small. NASA has pursued efforts to develop an ESP for Martian dust control and has reported positive results on the method's feasibility in the Martian environment.[1,2,3]

By integrating the cyclone with an ESP, the TSDS leverages the strengths of each technology. The cyclone stage addresses the large particles that are challenging for the ESP to extract, and the ESP is optimal at separating the fines that the cyclone is unable to stop. The cyclone reduces the concentration of particles that the ESP sees, which helps to maintain high efficiency in the ESP and reduce the rate of buildup of collected particles on the electrodes. While both technologies are scalable to large installations, cyclones scale better in terms of space-flight constraints. ESPs require larger collector areas as the flow rate is increased. Using a cyclone in the first stage can minimize the growth required of the electrostatic stage for larger-scale systems.

A. Cyclone Model

We developed an analytical modeling tool to predict the cyclone stage performance for different geometries and flows representative of Martian ambient conditions. Despite their widespread use in the industry, cyclone design remains a somewhat empirical art with customization to specific applications necessary for best performance. Because the flow and gas-particle interactions are complex, it is a difficult system to model, and model results must be verified with experiment. Further, models that are shown to work well for one range of geometries and flow conditions can be inaccurate when extended to different scales or flows. Little work has been done in the literature using cyclones in a low-pressure environment, so we sought to develop a tool that is applicable to the operation of a cyclone on Mars and can be used to guide system optimization. The key goals of the cyclone model are to predict pressure drop performance and separation efficiency. Separation efficiency usually scales with gas velocity in the cyclone, but the pressure drop has proven difficult in the literature to accurately predict. Thus, one of our main goals was to develop a model that would help us understand if a cyclone in a Martian environment could operate at high separation efficiencies within the tight < 2 torr pressure drop limitations.

For the analytical model, we leveraged a cyclone model developed by Bohnet and Lorenz,[8] which was an extension of earlier work by Mothes and Loffler.[9] We selected the Bohnet-Lorenz model because it incorporates includes the impact of changing gas properties via a Reynolds number-based friction factor correlation, whereas most other literature-based approaches that we reviewed ignore gas properties. In their discussion of optimization of small-scale cyclones, Salcedo et al.[10] also implemented the Bohnet-Lorenz model and found it to match the closest over other models with the optimized geometry in Salcedo's experiments.

The Mothes-Loffler/Bohnet-Lorenz model treats the cyclone as a cylinder with an equivalent volume to the actual cyclone geometry (shown in Figure 2). It assumes that the tangential velocity of the gas does not change in the axial direction and that the concentration of the particles is uniform in the radial direction for a given axial location. The cyclone is represented by four regions:
1. An entrance region defined by the annular section created by the outlet tube extending into the cyclone body.
2. The downward-flowing, outer vortex region that is characterized by particle flux toward the wall and by convective and diffusive particle and gas exchange with the upward-moving, inner vortex (Zone 4).
3. A region that captures the back-mixing and re-entrainment of already-deposited particles (requiring an assumed particle re-entrainment flow rate).
4. The upward-moving, inner vortex.

Additional key assumptions in the model are:
- A particle diffusivity term, set to 0.0125 m^2/s based on correlations developed by Mothes and Loffler and fitting to their test data, that influences the bypass exchange between the downward, outer vortex and upward, inner vortex.
- The re-entrainment zone is modeled by assigning a percentage of particles that bypass the cyclone.
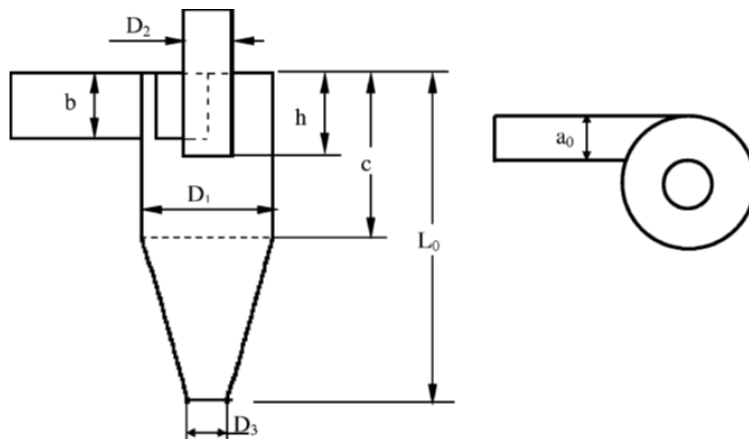

Figure 2. Key cyclone dimensions.

Particle removal is tracked in each section, and once particles reach the wall, it is assumed that they are collected except for the terms that explicitly address particle re-entrainment. The key extension that Bohnet and Lorenz made to the baseline model from Mothes and Loffler is to adapt the friction coefficient from an assumed constant to a

value dependent on gas properties. This friction factor is based on an empirical fit to their pressure drop data that incorporates the Reynolds number, predominately focused on performance over a range of increasing temperatures. Bohnet showed that this provided good correlation of pressure drop vs. flow rate at high temperatures.

We implemented the pressure drop and collection efficiency model and compared the predicted performance of a prototype cyclone to a pressure drop and particle collection experiment we performed in our laboratory. We used the experimental results to update the coefficients in the model, and compared final model predictions to computational fluid dynamics (CFD) simulations.

B. Experimental Measurements of Low-Pressure Cyclone Performance

1. Cyclone Prototype.

To validate our cyclone model, we performed flow pressure drop measurements and particle separation tests on a prototype subscale cyclone with a diameter of 1.26 inches and a total length of 4.9 inches. For convenience, we used an aluminum cyclone prototype from a previous project at Creare that was fabricated to separate dust in a pneumatic dust conveyance test facility. The prototype is on the same scale as would be needed for a ~0.090 kg/hr demonstration-class ISRU system (such as Mars 2020). A picture of the cyclone is shown in Figure 3.
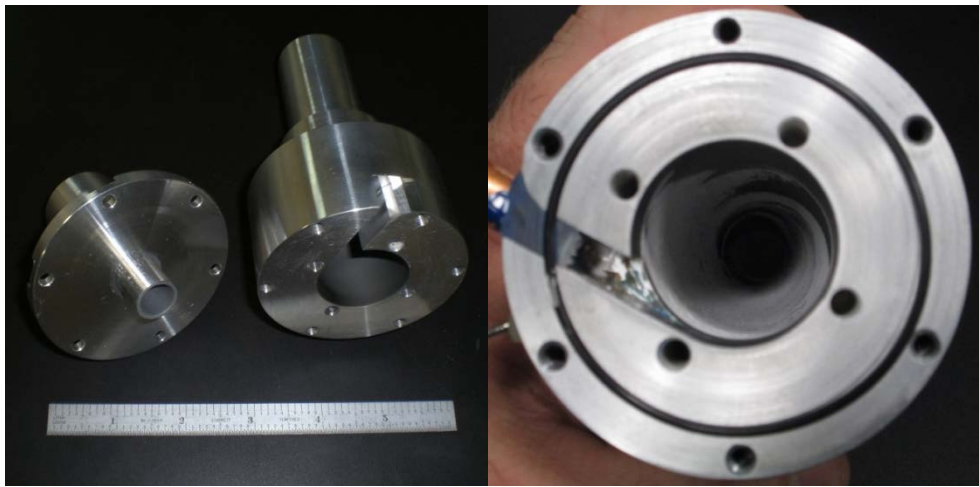

Figure 3. Prototype cyclone hardware (shown with vortex finder/top cap removed).

2. Dusty Gas Test Facility.

To test the cyclone, one of the key challenges was generating a dusty gas that could be sampled by the cyclone to simulate Martian atmospheric conditions. Our initial efforts to create a dusty atmosphere, low-pressure chamber were ineffective at keeping larger particles entrained, particularly at the low test flow rates of ~1 SLPM CO_2. The terminal velocity of 10 μm particles is around 1.5 cm/s in a 7 torr CO_2 atmosphere, and for particles larger than ~16 μm, it is higher on Earth in low-pressure CO_2 than on the reduced-gravity environment of Mars. Testing with larger particles is a key aspect of developing the TSDS, so we built a test facility that entrains dust particles in a high-velocity gas flow that is directed straight into the cyclone separator. By controlling the flow of dust into the gas stream with a hopper valve and adding vibration with a handheld engraving tool, we were able to achieve relatively controlled feed rates and successfully entrain samples with particles ranging from submicron to greater than 35 μm in low-pressure CO_2 flows. Figure 4 shows the dusty gas flow test facility with the cyclone, and Figure 5 shows an overall schematic of our particle separation testing that included Measurement Science Enterprise's (MSE) miniPCS particle sensor that provides both particle sizing and counting. Tests were performed by firstobtaining a baseline particle count with the cyclone removed from the flow path, using a consistent, measured mass of particles in the feed tube. Then, with the cyclone in place, tests were repeated, with an effort to maintain a consistent particle feed rate. The with- and without-cylone test particle counts were compared to estimate cyclone performance, along with the collected mass samples in the cyclone hopper and downstream HEPA filter.
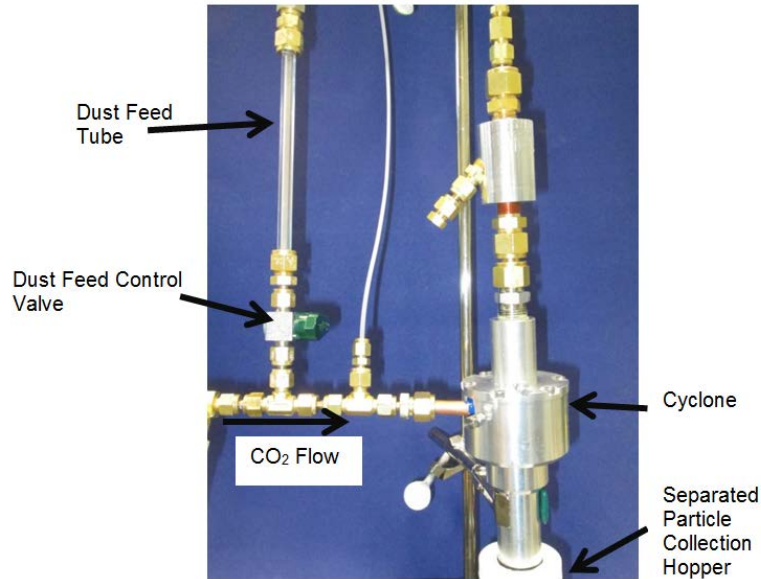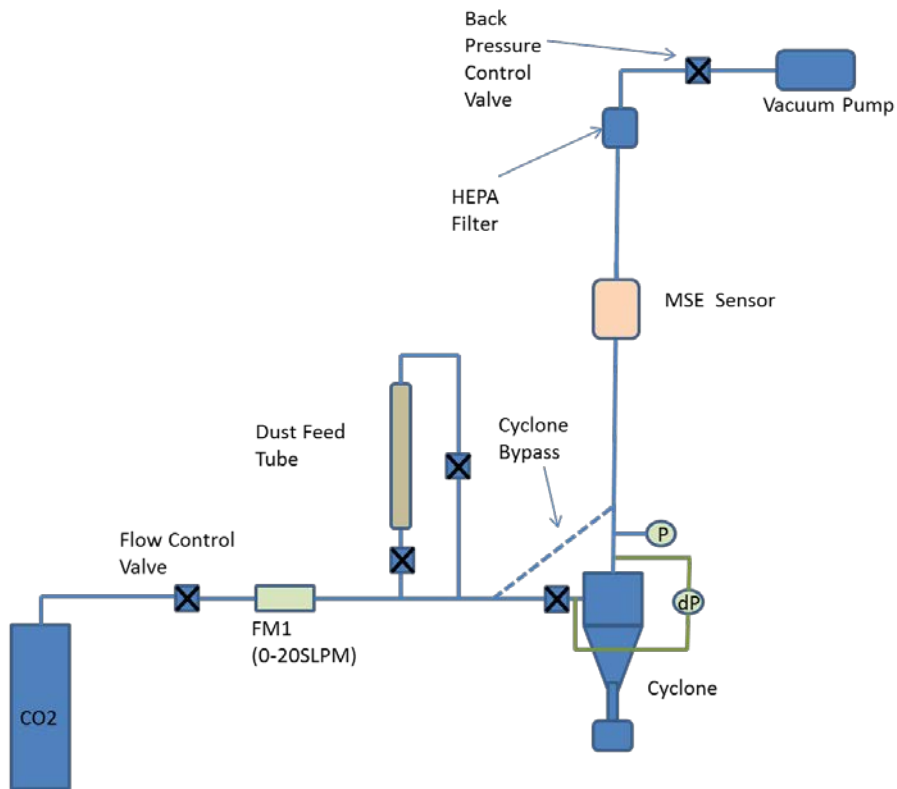
Figure 4. Dusty gas cyclone test facility.

Figure 5. Cyclone testing facility schematic with MSE particle sensor.

We installed pressure taps to the inlet and outlet ducts of the cyclone to measure the pressure drop across the cyclone over a range of inlet conditions from 50 to 300 torr cyclone outlet pressures. The taps were connected to a Magnehelic® differential pressure gauge with a range from 0 to 2.0 inches of H_2O (0 to 3.7 torr).

3. Experimental Pressure Drop Measurements at Martian Conditions.

We were unable to obtain accurate pressure drop measurements across the cyclone at the 7 torr Martian environment pressures due to small vacuum leaks in our test facility. In the interest of saving facility development

time, we had adapted the cyclone prototype to our low-pressure applications from a facility originally run at ambient conditions. The adapted system included an off-the-shelf filter assembly used after the cyclone to collect any remaining dust particles, as well as some plastic components used to create a dust collection hopper that was easy to remove, measure, and clean. These two items proved difficult to fully seal in a < 10 torr environment, and the small leakage flows were enough to swamp the measurement of very small pressure drops across the cyclone. However, the key result of this effort was that at 7 torr, the CO_2 flow rates needed to create a ~20 m/s cyclone inlet velocity that would result in higher separation efficiencies generated a pressure drop of less than ~0.5 torr, which was the measurement taken with the contribution of the leakage flow.

4. Experimental Pressure Drop Measurements at Higher Outlet Pressures (50 to 300 torr).

Due to the inherent difficulties of accurate cyclone modeling, it is desirable to use experimental data to inform and help develop the model. Since we could not adequately measure pressure drops at the lowest flow pressures, we performed a series of experiments at pressures ranging from 50 to 300 torr across a range of inlet velocities and mass flow rates. These tests fell into two categories:

- A set of measurements taken at a cyclone outlet pressure of 50 torr, where the mass flow rate was varied from 6.0 to 9.0 SLPM5 of CO_2. This produced inlet velocities to the cyclone ranging from ~15 to 24 m/s, which is in the range predicted to achieve high separation efficiency in the cyclone. It generated changes in the Reynolds number by changing the mass flow rate. The key factor in cyclone separation efficiency is achieving as high velocity as allowed within pressure drop constraints.
- A set of measurements taken at cyclone outlet pressures ranging from 50 to 300 torr at a nominal flow rate of ~9.5 SLPM. This data set allowed us to vary the inlet Reynolds number and gas velocity (from 4 m/s to 23 m/s) by adjusting the gas density.

These two data sets allowed us to explore the sensitivity of the cyclone and model to changes in gas density vs. flow rate. While there is still error present in these measurements (which we estimate to be ±0.5 torr), the overall trend between the measurements and the model were similar. The original computation of the pressure drop coefficient presented by Bohnet and Lorenz included correlations from their data, defining the pressure drop coefficient as presented in Equation (1).

$$K = \frac{\Delta P}{.5*\rho*v^2} = k_{in} + 0.8*\left(2 + 3*\left(\frac{U}{v}\right)^{\frac{4}{3}} + \left(\frac{U}{v}\right)^2\right) \tag{1}$$

where:
K = overall pressure drop coefficient
ρ = gas density
v = average exit velocity
U = outlet tangential velocity, which is a function of the friction factor and cyclone   surface areas (see Bohnet and Lorentz for further details)
k_{in} = inlet pressure drop coefficient (which was found to be   much smaller than the outlet coefficient)

Figure 6 and Figure 7 show the comparison between the model predictions and the two sets of measurements (measurements are corrected for dynamic pressure differences to show static pressure change). While the trends were very similar, the original Bohnet-Lorenz model resulted in overall higher pressure differences than measured. The source of this offset requires further investigation. Our tests were performed at a lower range of Reynolds numbers than the initial data that the friction factor correlations were based on, which could be the primary source of error. Testing at atmospheric conditions and varying temperatures would provide comparable conditions to those of Bohent. Applying a correction factor to the overall pressure drop coefficient of 0.3875 brings the model predictions in close agreement with the low pressure measurements. In both cases, the pressure drop increases with increasing flow velocity, as expected. We continued to use the adjusted pressure drop model using the correction factor ($K_{cor} = K*0.3875$) to support the trade study, but further experiments are necessary for true validation.

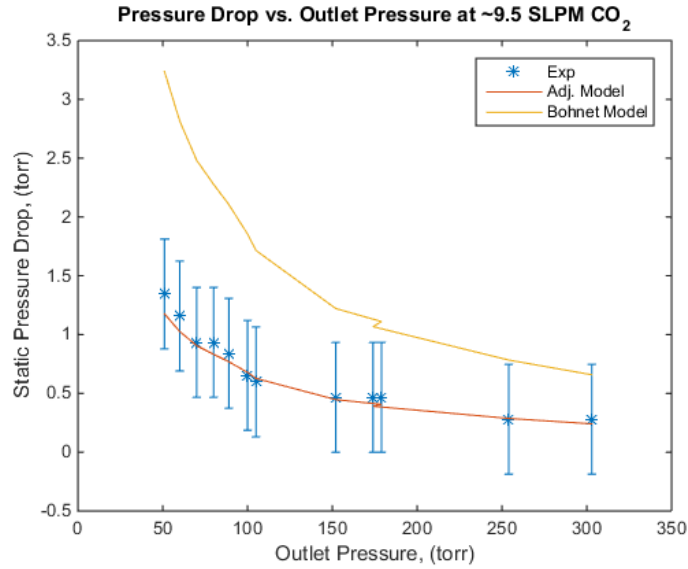[5]STP for the flow meter defined as 25°C at 14.7 psia

Figure 6. Comparison between pressure drop measurements and analytical model predictions for varying outlet pressures at a nominally constant mass flow rate (inlet velocity ranging from 4-23 m/s), showing original model and with low-pressure correction factor applied. *Note the variation in the model curves is due to small variations in the experimental flow rates used as inputs to the model).*
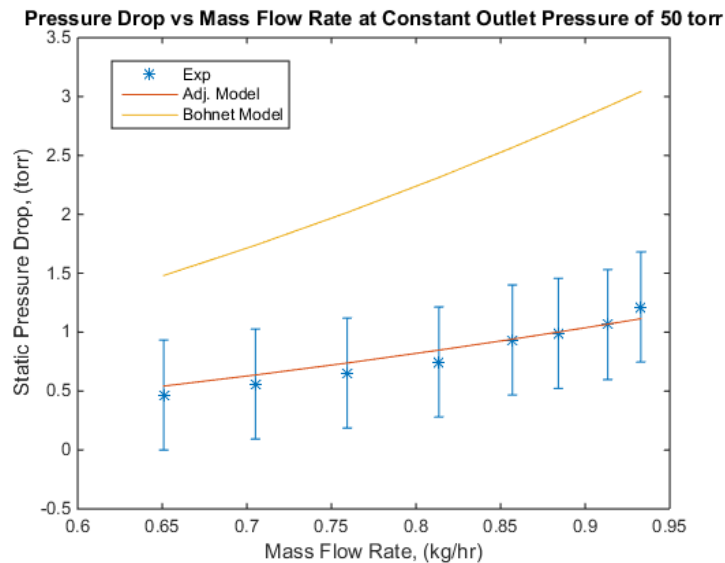

Figure 7. Comparison between pressure drop measurements and analytical model predictions for a constant outlet pressure of 50 torr with varying mass flow rates (showing original model and with a correction factor applied).

5. CFD Simulations of Cyclone Pressure Drop.

To estimate pressure drop performance under Martian conditions, we extrapolated the analytical model and applied it to the low-pressure Martian flow conditions of 7 torr at ~20 m/s inlet velocities necessary to achieve high particle separation efficiency. Because we could not compare the model to low-pressure measurements, we performed CFD simulations to both visualize the flow and gain additional confidence in the predicted pressure drop through the cyclone at Martian pressures.

The CFD simulations were conducted for a range of mass flow rates at a 7 torr outlet pressure as well as the higher outlet pressures cases where measurements were taken. The low outlet pressure cases correspond to laminar flow conditions with very low inlet Reynolds numbers of less than 250. Transition to turbulent flow occurs in the Reynolds number range of about 1,500 to 2,500. With the higher densities at the 50 to 300 torr cases, the Reynolds

International Conference on Environmental Systems

numbers for these conditions range from 1,200 to 2,000, placing them right in the transitional flow regime. Methods for modeling laminar and turbulent flows in CFD vary considerably. Generally, laminar flow simulations are much simpler and more accurate than turbulent flow simulations. We performed a laminar flow simulation for the 7 torr cases, and a turbulent simulation for the > 50 torr cases.

Turbulent flow simulations rely upon turbulence models to capture turbulent diffusion of momentum in the flow field. The applicable CFD model that offers computationally tractable solution to turbulent flow fields in cyclones is the Reynolds stress equation model (RSM). The RSM captures anisotropic turbulence prevalent in flow fields with significant swirl complex strain fields, whereas more common models assume isotropic turbulence (e.g., k-omega and k-epsilon models).

The results of the CFD simulations are shown in Figure 8 and Figure 9. Note that here we are comparing the static pressure drop since the static pressure was measured experimentally. The total pressure drop computed by the CFD is shown for reference. For the transitional/turbulent cases, the results indicate that the pressure drop predicted by the CFD model is only about half of the measured value. However, the trends are captured very well. For the laminar, Martian pressure cases, the CFD analysis lines up very closely with the analytical model predictions.

Further analysis would be required to determine the source of the discrepancy in the CFD simulations between the laminar and transitional scenarios, but the key result from this effort is that the analytical model predicts the correct trends in pressure drop, and the overall magnitude of the pressure drop through the cyclone is much lower than the 2 torr constraint imposed by an ISRU blower.
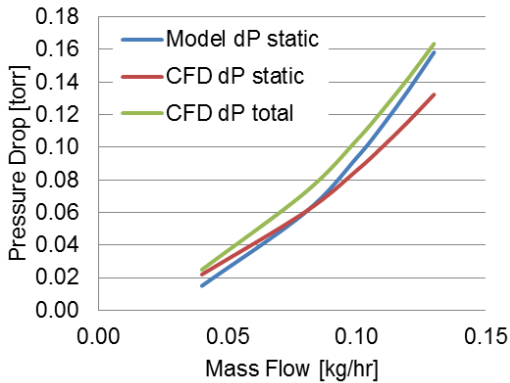

Figure 8. Pressure drop predictions at Martian conditions: comparing CFD laminar analysis to analytical model results.
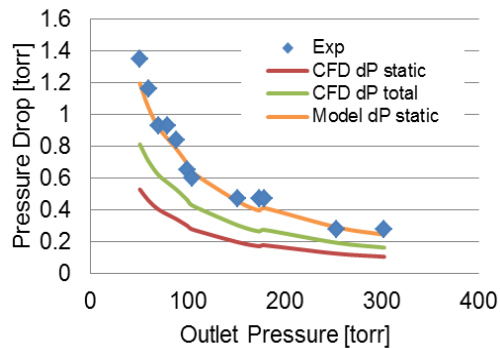
Figure 9. Pressure drop predictions at higher pressures: comparing CFD turbulent analysis to analytical model results and experimental data.

6. CFD Visualization of Flow Patterns.

We also used the detailed CFD results to evaluate assumptions used in the first-order cyclone model, namely the tangential velocity profile. The analytical model assumes that the velocity tangential velocity profile is constant with axial location and radially decreases from the inner vortex edge toward the outer wall. The contour plots of tangential velocity in Figure 10 and the path line plot in Figure 11 show that the assumption is qualitatively valid in the cylinder region of the cyclone. In the cylinder region of the cyclone, the tangential velocity is largely in the range of 5 to 8 m/s, with the exception of the high-velocity inlet region. Below the cylinder in the cone region, the tangential velocity is very small and the axial variation assumption does not hold. The velocity drops off in the cone region because most of the flow is entrained into the exit flow in the cylinder section of the cyclone prior to entering the cone section. The path lines in Figure 11 represent the path of a massless particle in the flow field. Only a small fraction of the massless particles released from the inlet surface penetrate into the cone region. This result indicates that the cyclone length should be shortened, and trade-offs between diameter and cylinder length should be explored in future research for enhancing the flow length and thus particle residence time within the cyclone. These findings will be used in future research to extend the analytical model by adjusting how the bypass flow from outer-to-inner vortices is calculated.
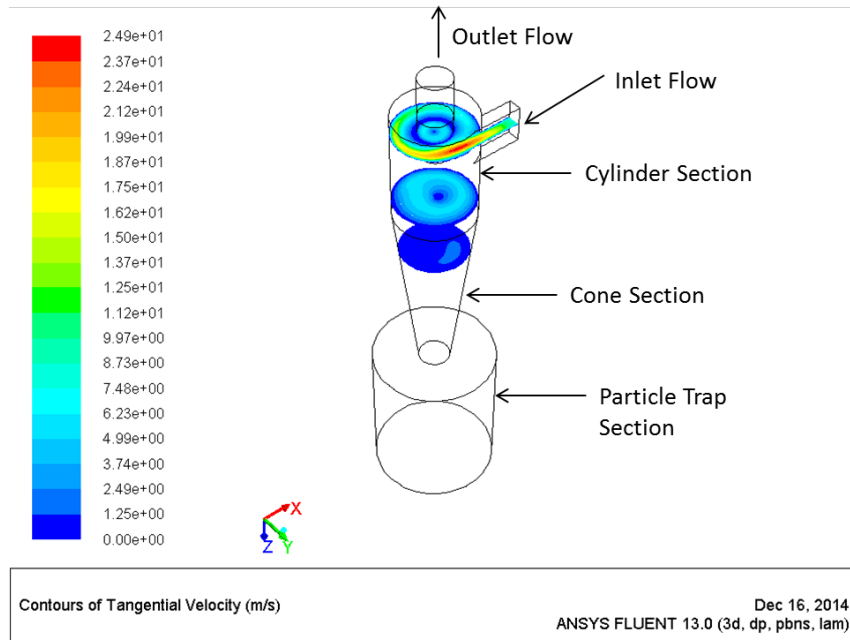
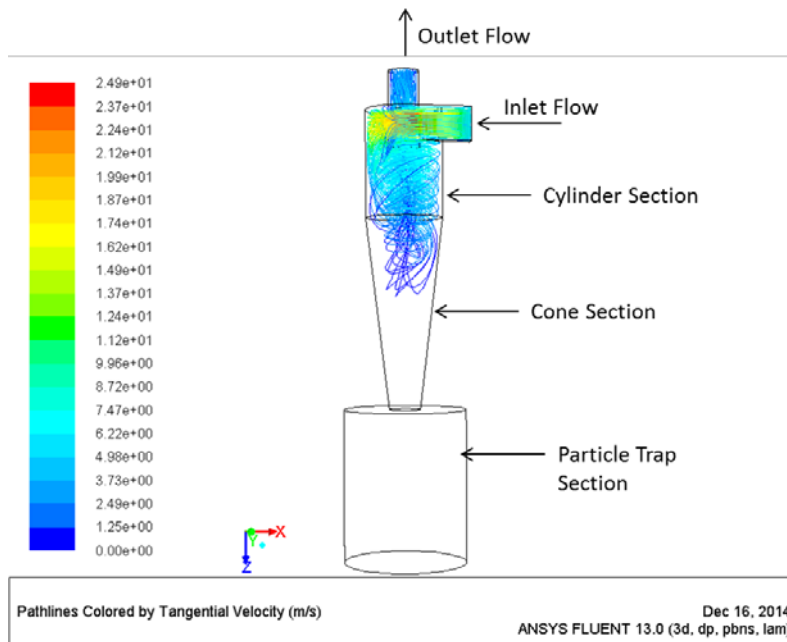**Figure 10. Tangential velocity on three parallel radial planes.**

Figure 11. Flow path lines show that the vortex does not significantly penetrate into the cone section of the cyclone.

7. *Separation Efficiency Modeling and Measurements.*

The second primary goal of the analytical cyclone model is to estimate the separation efficiency of a given cyclone geometry for a given set of flow conditions. The modeling approach was described in Section IIA, with additional details available in Bohnet and Lorenz[8] and Mothes and Loffler.[9] We performed a series of dust separation experiments using one of MSE's standard miniPCS particle detectors to measure the distribution of a dusty gas flow both without the cyclone separator and with the cyclone separator. For dust simulant, we used both spherical glass beads with a mean diameter of 10 μm and a maximum diameter of ~32 μm, as well as a sample of JSC-1 Mars simulant (predominatly for demonstration purposes). Because only one miniPCS sensor was available,

the tests were run in series—first flowing dust through the system without the cyclone, then flowing with the cyclone, sampling for the same period of time in each test. The resulting particle count distributions were normalized by the mass of dust input to each run and the particle count per bin per gram, but variations in achieving consistent concentrations of dust entrainment make it difficult to do a complete comparison of cyclone performance. In future work, we will integrate two particle sensors into the test facility to acquire in situ before and after measurements of the dusty gas flow through the separation system.

All particle separation tests were performed at a cyclone inlet pressure of 13 torr and a CO_2 flow rate of 1.0 SLPM (0.11 kg/hr CO_2). Because the existing form factor of the standard miniPCS required a ¼″ ID flow line, integration of the MiniPCS into the test facility resulted in more flow resistance than was present for the flow pressure tests. As a result, the laboratory vacuum pump could not pull the system down to 7 torr at the desired CO_2 flow rates, and our separation measurements were performed at a lower cyclone inlet velocity of 10 m/s rather than the ~20 m/s that the model predicts is needed for high separation efficiencies. Thus, we expected our experiments to measure lower efficiencies than are expected under prototypical Martian operating conditions.

Figure 12 shows the distribution of particles before and after the cyclone using glass beads, and Figure 13 shows the test using the Mars JSC-1 simulant. From the count histograms, it can be seen that qualitatively the cyclone is performing well. The sources of error that contribute to the uncertainty of the result include sensor error (±10%) and the variation in the dust feed rate due to the limitations of the dust entrainment system. The MiniPCS sensor was only calibrated for use with the glass beads; the refractive index differences between the galss beads and Mars simulant were not taken into consideration in the measurements. Recognizing that Mars simulant is inherently difficult to size with a Mie-scattering probe due to nonspherical particles, the Mars simulant tests provided more of a qualitative demonstration of cyclone efficiency than characterization of the simulant.
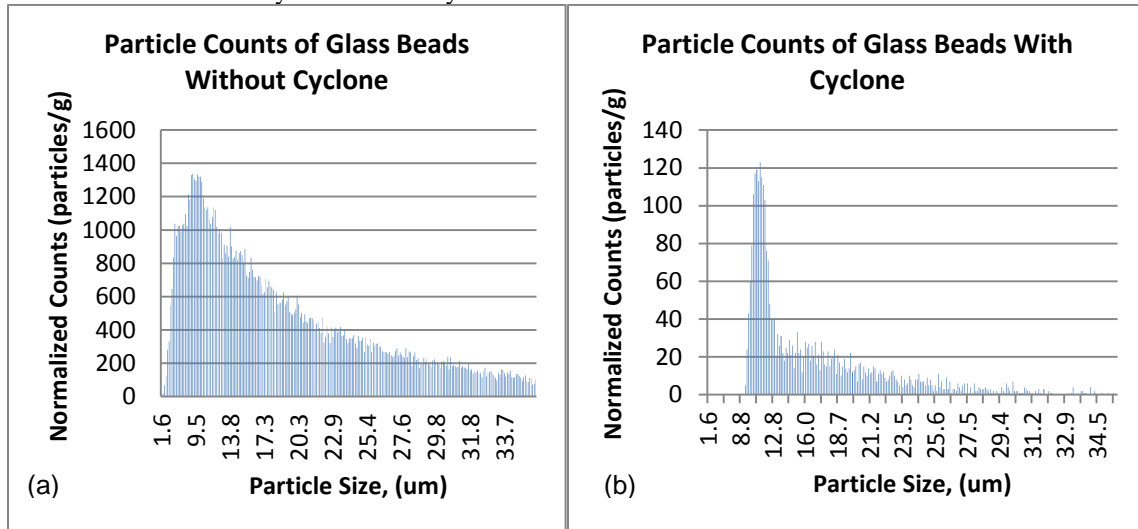

Figure 12. Particle distribution of glass beads detected (a) without cyclone separator, and (b) with cyclone separator.
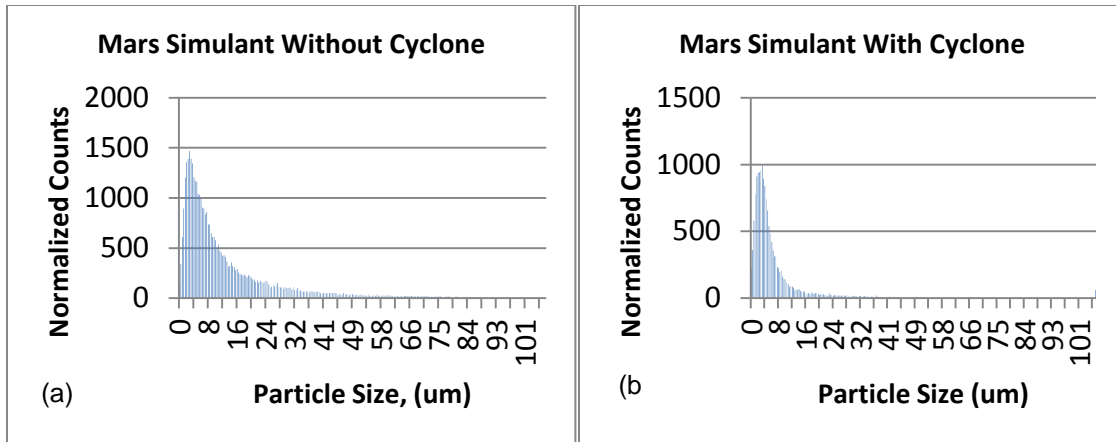
Figure 13. Particle distribution of mass simulant detected (a) without cyclone separator, and (b) with cyclone separator.

8. Model Separation Efficiency Predictions.

The analytical model separation efficiency prediction is shown with the experimental results in Figure 14. The model matches well with the glass bead experiment but significantly over-predicts the separation efficiency measured in the Mars simulant experiment. The size distribution of the glass beads did not have enough particles less than 10 μm to fully map out the efficiency curve, but the cyclone performed very well in separating the larger particles. The cyclone performs significantly worse for the Mars simulant than for the spherical glass beads; several factors weigh into this result:

- The particle sensor itself becomes much less accurate with nonspherical particles, and the Mars simulant particle shape is less uniform than the glass beads, so this will add to size detection errors.
- The particle sensor was not calibrated for the difference in refractive indices between the glass beads and the Mars simulant.
- With nonuniform particles, the particle aerodynamic diameter may be lower, requiring a longer residence time in the cyclone in order for those particles to migrate radially through the gas stream to the wall before the flow enters the inner vortex.

Because these tests were performed at a slower velocity than the ideal cyclone inlet, we believe the efficiency can be increased by increasing the velocity through the cyclone, and our pressure drop analysis has shown that this is viable to do and still remain within the overall pressure drop constraints. Further experiments and refinement of the test facility will aid in refinement of the separation model; however, it serves as a useful design tool that captures the predominant behavior of the system.

Based on the pressure drop predictions of the analytical model, we could increase the cyclone inlet velocity from the ~10 m/s of the particle separation tests up to > 50 m/s and still remain under a 2 torr pressure drop. With optimization of the cyclone geometry and generation of higher flow velocities, a separation efficiency of 90% of 1 μm particles should be feasible.
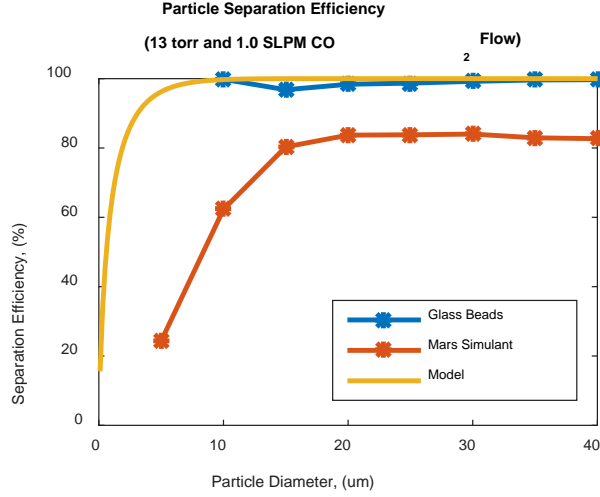
Figure 14. Model separation efficiency for subscale test cyclone compared to experimental results.

C. Electrostatic Precipitator Modeling

The second part of our model development effort entailed creating a design and analysis model of an ESP to develop an understanding of how the system scales with varying flows and particle separation targets. The combined analysis of the ESP and the cyclone allow us to understand where the trade-offs between the two stages exist and what an optimized, integrated two-stage separator would look like.

We modeled an ESP using a cylindrical configuration, and following the analysis approach discussed by Parker[11] and the model development for low-pressure Martian ESPs that has been presented by Calle et al.[2] Because the modeling equations are laid out in detail in these two references, we will not repeat them here. The cylindrical ESP configuration consists of a single discharge wire running along the axis of a tube through which the gas flow travels. The inner surface of the tube serves as the grounded collector electrode. In an ESP, a high voltage is applied to the discharge electrode, creating a strong electric field between the wire and the tube wall. As gas flows through the system, a corona of ionized gas molecules develops around the discharge electrode, electrostatically charging the aerosol particles entrained in the flow. Once charged, the particles are drawn by the electric field toward the tube wall where they remain stuck through a combination of electrostatic and van der Waals forces. To achieve a high collection efficiency in an ESP is a balance between the strength of the electric field between the two electrodes (by increasing the voltage) and the flow length—a longer flow path allows more time for a particle to drift to the collector wall, driven by the force of the electric field. Terrestrial ESPs often operate at > 20 kV, but the particular challenge of operating an ESP in Martian atmospheric conditions is that the breakdown voltage (where a discharge arc is generated) in low-pressure CO_2 is very low—on the order of 1 to 5 kV, depending on the spacing between the two electrodes. An ESP must operate between the corona on-set voltage and the breakdown voltage. This limitation drives the Martian ESP to be longer in order to achieve high particle separation, particularly for larger particles.

We are predominantly investigating the ESP for use with particles less than ~5 µm in diameter. To determine if the flow regime for gas-particle interactions in our range of interest, we plot the Knudsen as defined in Equation (2) in Figure 16. For Knudsen numbers (Kn in) << 1 the flow is considered continuum flow, = 1 is transitional, and >> 1 is molecular flow.

$$Kn = \frac{2\lambda}{d} \tag{2}$$

where λ is the mean free path in the gas and d is the particle diameter.

For Martian conditions of CO_2 at -50°C and assuming an inlet pressure to the ESP of ~5 torr (after the cyclone stage), the mean free path is calculated from Equation (3), using references of Tr = 273.15 K, Pr = 1 bar, Sutherland constant (S) = 220.5 K and λr = 44 nm (CO_2 at STP).[12]

$$\lambda = \lambda_r \cdot \frac{T}{T_r} \cdot \frac{P_r}{P} \left(\frac{1 + S/T_r}{1 + S/T} \right) \tag{3}$$

This yields a mean free path of CO_2 at 5 torr and -50°C of 4.6 µm. Figure 15 shows the Knudsen numbers are greater than one for all sizes < ~8.3 µm particles. This indicates that gas-particle interactions are predominantly in

the molecular flow regime, entering into transitional flow as the particle sizes approach ~5 μm. This flow regime requires modification of Stoke's law with the Cunningham slip correction factor when expressing the drag force on the particles. Because the mean free path of the gas molecules' free path is large compared to the particle size, there is a significant "slip" between gas and dust particles. Note that the Knudsen number for the gas flow, using flow channel hydraulic diameter, is much smaller than one; thus, gas flow analyses in both the ESP and the cyclone stage can be treated as laminar, continuum flow. However, it is the gas-particle interaction that falls in the transitional-to-molecular regimes. In the molecular flow regime and for particles < 1 μm, particle charging is dominated by the diffusion charging mechanism, whereas in a continual flow regime and for larger particles, charge accumulation is dominated by field charging.
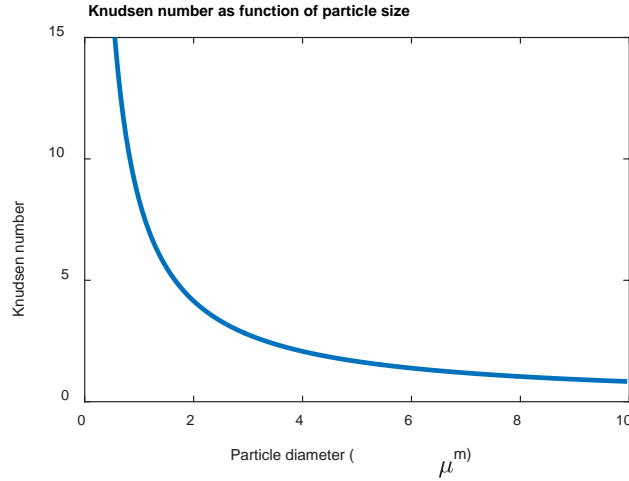
Knudsen number as function of particle size

Figure 15. Knudsen number as a function of particle diameter at 5 torr and -50°C.

There are many models to describe the rate of charge accumulation across these two regimes, and because we are interested in a particle size range that spans both mechanisms, we elected to use the model developed by Cochet as presented in Parker[11] that defines a continuous charging process across the particle size range in an analytical form. This is presented by the particle saturation charge in Equation (4) and the time-dependence in Equation (5), using the time constant, τ_Q, defined by Equation (6). This approach may overestimate the charge buildup on particles in the transitional regime, ~1 μm – 10 μm, and thus may overestimate ESP collection efficiency.

$$Q_p^\infty = \left\{ \left(1 + 2\lambda/d_p\right)^2 + \left(\frac{2}{1+2\lambda/d_p}\right)\left(\frac{\varepsilon_r-1}{\varepsilon_r+2}\right) \right\} \pi \varepsilon_0 d_p^2 E \tag{4}$$

$$Q_p(t) = Q_p^\infty \frac{t}{t+\tau_Q} \tag{5}$$

$$\tau_Q = \frac{4\varepsilon_0}{j/E} \tag{6}$$

where: Q_p^∞ = saturation charge of particle (C)
$Q_p(t)$ = charge on particle after time t (C)
D_p = particle diameter (m)
ε_r = particle relative permittivity
ε_0 = vacuum permittivity (F/m)
E = electric field strength (V/m)
j = ESP current flux (A/m^2)

The inputs to our ESP model include discharge wire and flow tube diameter, tube length, gas type, temperature, pressure, flow rate, and applied voltage across the ESP. The model determines the electric field as a function of radius within the flow tube and incorporates space charge effects. The charge buildup on a particle varies with particle diameter and the ion density of the corona. The radial migration velocity, w, of the particle toward the tube wall is a function of its charge, diameter, and the electric field strength. The precipitator collection efficiency, η_{esp} is defined by Equation (7).

$$\eta_{esp} = 1 - e^{-\left(\frac{A}{\dot{V}}\right)w} \tag{7}$$

where A is collection area (m^2) (perimeter of the tube time the length) and $\dot{V}$ is the gas flow rate (m^3/s).

To maximize the performance of the ESP, it must be operated at as high an applied voltage as possible while staying below the electrical breakdown voltage of the gas. For our system-level analysis, we operate the ESP at 85% of breakdown voltage to provide some margin against initiating a discharge arc. The performance of the ESP then becomes a trade between tube radius (flow area), flow length, and particle collection efficiency requirements. A larger tube radius means that a particle has a longer radial distance to drift before collecting on the wall, but this is counteracted by the lower flow velocity for a given mass flow rate of gas and the higher electric field that can be employed across the larger electrode gap. Figure 16 shows the breakdown voltage under Martian conditions as a function of tube diameter,[2] and Figure 17 shows collection efficiency curves of a 3 inch diameter (7.62 cm) ESP for varying tube lengths at a CO_2 flow of 1.8 kg/hr (equivalent to a validation-class ISRU mission production rate). From Figure 17, it is clear that the ESP performs much better for smaller particles.
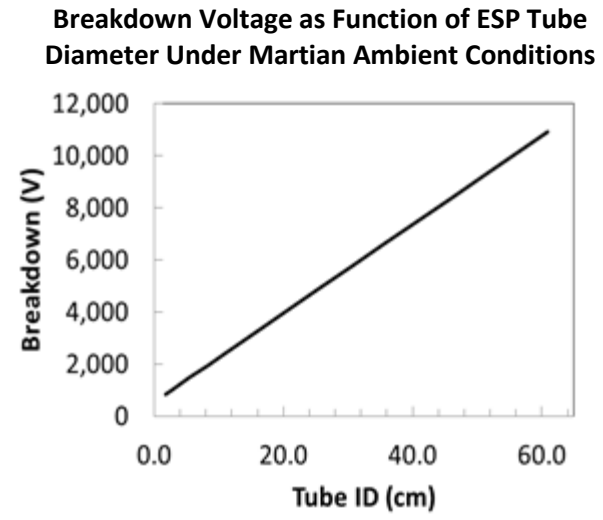

Figure 16. Breakdown voltage as a function of tube ID for a cylindrical ESP operating in Martian ambient conditions.
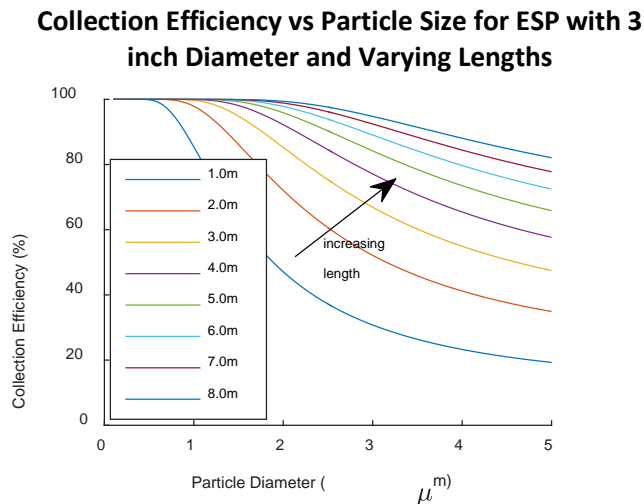

Figure 17. Collection efficiency as a function of particle diameter for varying ESP lengths at a tube diameter of 7.62 cm (3 inches) for 1.8 kg/hr CO_2.

Figure 18 shows the tube length required to achieve a separation target of 90% of 5 μm and of 1 μm particles for varying tube diameters. This result shows that for a single-stage dust separation system capturing particles up to 10 μm using only an ESP, the ESP would need to be very large, even at the validation-class mission level—it would

probably need to employ parallel tube banks to reduce the flow velocity and have a long flow length. In addition, an ESP sized to handle the full particle size range will consume much more power. The ESP size requirements to separate only particles ≤ 1 μm are much more reasonable.
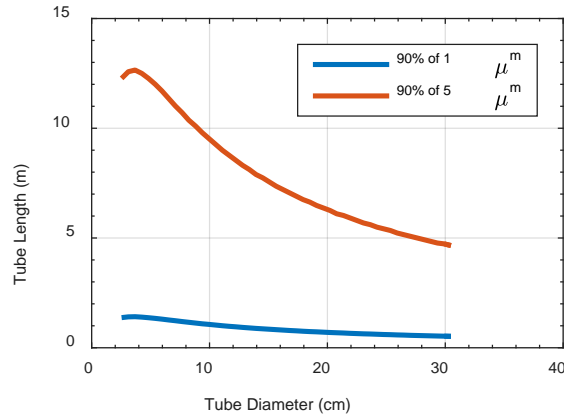

Figure 18. ESP tube length vs. tube diameter required to collect 90% of 1 μ and 5 μm particles at CO_2 flow of 1.8 kg/hr.

D. System-Level Model Results

The models for the two stages of the TSDS were combined to produce system-level performance and sizing estimates for a validation-class ISRU mission with CO_2 flow rates of 1.8 kg/hr. Based on modeling results from the individual stages, to achieve an overall separation efficiency requirement of 99% for particles ≥ 0.3 μm in diameter, we defined the individual stage separation requirements as:

- Cyclone: η ≥ 90% for particles ≥ 1.0 μm.
- ESP: η ≥ 90% for particles ≤ 1.0 μm.

This results in a total separation efficiency of > 99% for the full particle range. While we did not have time to perform a full optimization study of cyclone geometries, we used the cyclone model to select a design that meets our performance goals for the validation class mission. Our preliminary sizing estimates for a validation-scale cyclone separator predict that a cyclone on the order of 8.9 cm (3.5 inches) in diameter and 23 cm (9 inches) long can achieve high separation efficiencies down to less than 1.0 μ particle size with a pressure drop of 1.0 torr. Figure 19 shows the predicted separation performance of the cyclone first stage. This is not an optimized design—optimization of the cyclone geometry and further experiments may allow the cyclone size to be reduced.
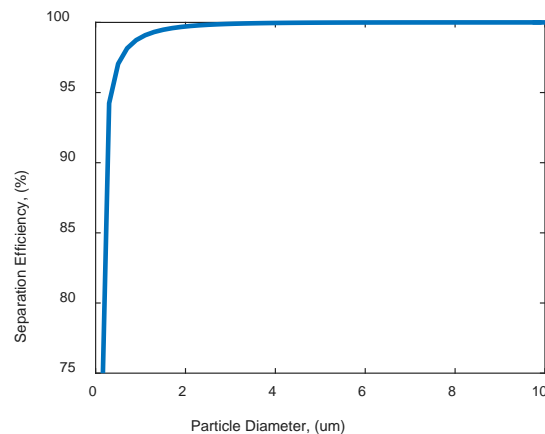

Figure 19. Validation-class mission cyclone separation efficiency. *A 9 cm diameter x 23 cm long cyclone can achieve > 95% collection of particles ≥ 1.0 μm for CO_2 flows = 1.8 kg/hr and a pressure drop of 1.0 torr under Martian ambient conditions of -50°C and 7 torr.*

With the separation requirement for the ESP stage reduced to addressing the submicron to 1.0 μm range, the size of the ESP can be drastically reduced. Figure 20 shows the trade between ESP length and diameter to achieve 90%

collection of 1 μm particles, and Figure 21 shows the collection efficiency across the particle size range for an ESP 8.9 cm (3.5 inches) in diameter for different ESP lengths. Selecting an ESP stage that is 1.1 m long and 8.9 cm in diameter to combine with the cyclone yields a two-stage, regenerable separation system sized for a validation class mission that can separate out 99% of particles across the full size range that may be required for Mars operation. Figure 22 shows the combined collection efficiency of the TSDS. The pressure drop through the ESP stage is negligible, so the predicted total pressure drop through the system is on the order of 1.0 torr. The ESP model uses the cyclone output pressure as an input to determine gas flow properties in the ESP. The predicted ESP power consumption is less than 1 W.
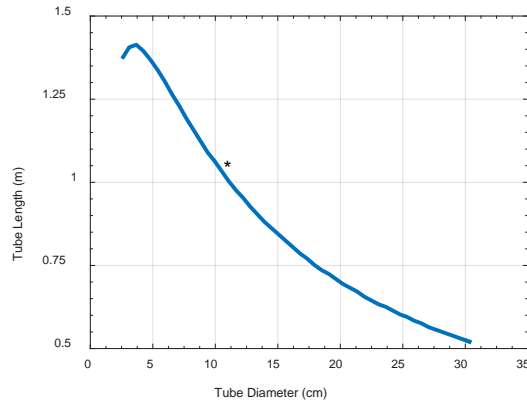

Figure 20. ESP length vs. diameter required for 90% collection efficiency for 1.0 μm particles. *A diameter of 11 cm is required to reduce the length to 1.0 m.*

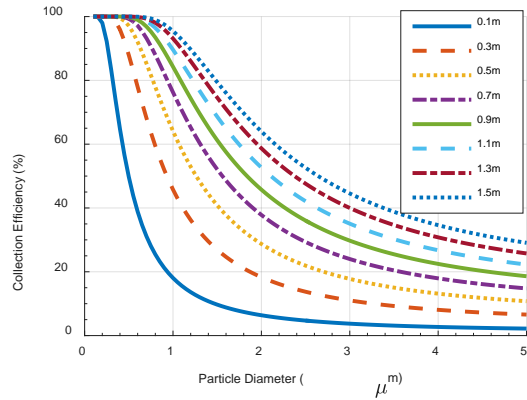**Figure 21. ESP collection performance.** *A 8.9 cm (3.5 inch) diameter ESP must be 1.1 m long to collect 90% of 1.0 μm particles.*
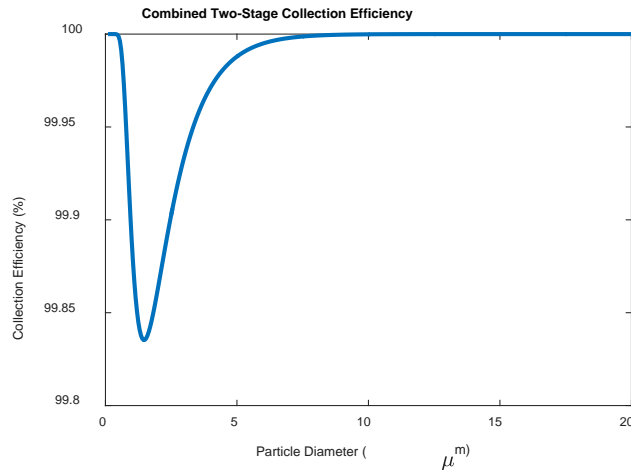
Figure 22. The combined collection efficiency of the two-stage dust separator.

Integration of the two stages will require some design considerations. Minimizing the ESP length requires higher voltages and thus larger diameters to avoid breakdown in the low-pressure gas. Expanding from the smaller outlet tube of the cyclone stage to a large diameter ESP will require intelligent diffuser design. Recent literature on cyclone performance optimization has discussed the design of diffusers that convert the rotational energy in the exiting cyclone flow back to static pressure (potential energy), reducing the cyclone pressure drop[13]. Such an implementation can also help the flow expansion into the ESP stage. Additional considerations will include the removal of dust from each stage. Typically this is accomplished with rappers, in the case of the ESP stage, to vibrate the collection electrode and cause dust to fallinto a collection area. A combination of this and pulsed, back-flowing gas jets may help reduce particulate buildup within both the ESP and cyclone. The ESP flow entrance may need to be designed to avoid interference with dust removal. Other ESP implementations such as a wire-plate approach may prove easier to clean the collector surfaces.

III.   Conclusions

We have designed and modeled a two-stage Martian dust separator system for ISRU atmosphere processing plants that can achieve a collection efficiency of > 99% for all Martian particles with a low pressure drop. Our combined model presents the trade-offs in sizing an ESP for Martian operating conditions and illustrates the advantage of employing a pre-filter stage to separate large particles. We present an inertial cyclone as a viable first-stage separator that requires no moving parts and is regenerable simply by emptying the collection hopper. We developed a low-pressure cyclone model using experiment results to verify pressure drop predictions. The modeling tools we developed allow us to explore the design space of the integrated two-stage separator. These tools demonstrated that optimizing a cyclone pre-filter will greatly reduce the required size of a highly efficient, second-stage ESP. Our key conclusions are as follows:

- A cyclone pre-filter can be operated at velocities exceeding 20 m/s in Martian atmospheric conditions with < 1.0 torr pressure drop, which allows room for higher velocities and optimization of separation efficiency.
- A cyclone capable of 90% separation of particles greater than 1 μm will greatly minimize the sizing of the ESP.
- An ESP that targets particles < 1 μm can fit within a 8.9 cm (3.5 inch) diameter, 1.1 m long form factor and enable a system separation efficiency of 99% of all particles greater than 0.3 μm for a validation-class mission processing 1.8 kg/he CO_2.

A.   Recommended Next Steps

Forward work is required to continue model validation and to optimize the design of the TSDS. Refinements to the test facility to accommodate more accurate low-pressure cyclone experiments and testing several different cyclone geometries will aid in validation of the cyclone model. Using the model to do a more detailed exploration on the impact of various geometries and sizing parameters will aid in optimization of the cyclone geometry. The ESP model should be compared to experimental data for validation, and alternative ESP form factors, such as a parallel plate configuration, could be explored. Mechanical integration of the two stages should be developed to enable removal of dust from the collection zones and condition the flow between stages.

Acknowledgments

References

[1]Calle, C. I., Mackey, P. J., Hogue, M. D., Johansen, M. R., Kelley, J. D., Phillips, J. R., and Clements, J. S., "An Electrostatic Precipitator System for the Martian Environment," *Journal of Electrostatics*, Vol. 71, Issue 3, Jun 2013.

[2]Calle, C. I., Thompson, S. M., Cox, N. D., Johansen, M. R., Williams, B. S., Hogue, M. D., and Clements, J. S. "Electrostatic Precipitation of Dust in the Martian Atmosphere: Implications for the Utilization of Resources During Future Manned Exploration Missions," *J. Phys. Conf. Ser.*, Vol. 327, No. 1, Dec. 2011, p. 012048.

[3]Clements, J. S., Thompson, S. M., Cox, N. D., Johansen, M. R., Williams, B. S., Hogue, M. D., Lowder, M. L., and Calle, C. I., "Development of an Electrostatic Precipitator to Remove Martian Atmospheric Dust From ISRU Gas Intakes During Planetary Exploration Missions," *IEEE Transactions on Industry Applications*, Vol. 49, Nov 2013, pp. 2388–2396.

[4]Komguem, L., Whiteway, J., et al., "Phoenix LIDAR Measurements of Mars Atmospheric Dust," *Icarus*, Vol. 223, No. 2, 2013, pp. 649–653.

[5]Gross, F., Grek, S., Calle, C., and Lee, R., "JSC Mars-1 Martian Regolith Simulant Particle Charging Experiments in a Low-Pressure Environment," *Journal of Electrostatics*, Vol. 52, No. 4, Oct 2001, pp. 277–266.

[6]NASA Announcement of Opportunity, MARS 2020 Investigation, NNH13ZDA018O, revised Oct 21, 2013.

[7]Pennington, C., Sorensen, E., et al., "Inertial Filtration of Lunar Dust in Reduced Gravity," Joint Annual Meeting of LEAG-ICEUM-SRR, 2008.

[8]Bohnet, M. and Lorenz, T. "Separation Efficiency and Pressure Drop of Cyclones At High Temperatures," *Gas Cleaning at High Temperatures*, Clift et al. (eds.), Springer, Dordrecht, 1993

[9]Mothes, H. and Loffler, F., "Prediction of Particle Removal in Cyclone Separators," *American Institute of Chemical Engineers*, Vol. 28, No 2, 1998, pp. 231–240.

[10]Salcedo, R. and Candido, M., "Global Optimization of Reverse-Flow Gas Cyclones: Application to Small-Scale Cyclone Design," *Separation Science and Technology*, Vol. 36, No. 12, 2001.

[11]Parker, K. R. Ed., *Applied Electrostatic Precipitation*, 1996 edition. London; New York: Blackie Academic & Professional, 1997

[12] Schmid, O., Trueblood, M. B., Gregg, N., Hagen, D. E., and Whitefield, P. D., "Sizing of Aerosol in Gases Other Than Air Using a Differential Mobility Analyzer," *Aerosol Sci. Technol.*, Vol. 36, No. 3, pp. 351–360, Mar. 2002.

[13] Kahrimanovic, D., Puttinger, S., Aichinger, G., Pirker, S., "Minimizing Pressure Drop in Cyclone Separators-Measurements and Numerical Simulations", *11th World Filtration Congress*, April 16-20, 2012.

International Conference on Environmental Systems